ASME Journal of Engineering for Gas Turbines and Power
Online journal at:
https://asmedigitalcollection.asme.org/gasturbinespower

On a Novel Co-Rotating Synchronous Turbine Mode Operation in a Centrifugal Compressor

David John Rajendran
Rolls-Royce UTC,
Centre for Propulsion and Thermal Power Engineering,
Cranfield University,
Cranfield MK43 0AL, UK

Eduardo Anselmi Palma
Rolls-Royce UTC,
Centre for Propulsion and Thermal Power Engineering,
Cranfield University,
Cranfield MK43 0AL, UK

Ioannis Roumeliotis
Rolls-Royce UTC,
Centre for Propulsion and Thermal Power Engineering,
Cranfield University,
Cranfield MK43 0AL, UK

Vassilios Pachidis
Rolls-Royce UTC,
Centre for Propulsion and Thermal Power Engineering,
Cranfield University,
Cranfield MK43 0AL, UK

David Sayre
Rolls-Royce Corporation,
Indianapolis, IN 46225

Nicholas Howarth
Rolls-Royce plc.,
Moor Lane,
Derby DE24 8BJ, UK

A novel co-rotating, synchronous, reverse flow (RF) turbine mode operation in a centrifugal compressor (CC) is investigated, and methods to enable this mode, its working principles, flow field features, and key performance characteristics are described. This is done by using three-dimensional (3D) Reynolds–averaged Navier–Stokes (RANS) flow field simulations on a simplified variant of the NASA High Efficiency Centrifugal Compressor (HECC) geometry, which represents a typical state-of-the-art design practice. The novel co-rotating turbine mode is elucidated by first considering the baseline contra-rotating, reverse flow turbine mode as would be expected from the conventional four-quadrant CC operation map. This baseline contra-rotating turbine mode is also hitherto undescribed in the literature for CC. Therefore, the flow field and performance metrics in the baseline contra-rotating mode are utilized to provide insights into the possibility of engineering design elements that can enable the novel co-rotating turbine mode. The novel co-rotating, turbine mode is found to be enabled by the introduction of a suitable swirl generation mechanism that will direct the flow onto the impeller wheel suction side to give it a rotational impulse to spin from the suction to the pressure side as in nominal operation. The flow expansion through the reversed impeller wheel flow path with radius reduction enables power production. In the novel co-rotating, turbine mode, the flow leaves the impeller wheel in the same direction as it enters because of the direction of rotation and impeller inlet flow angle. However, this does not significantly impact power production because of the reduced radius weighting of the absolute swirl at the impeller inlet. An exemplary co-rotating turbine mode enabling configuration with 45 deg rotated diffuser vanes is found to handle up to 46% higher reverse flow and yield 6.25% higher peak power output even with a 16% lower absolute swirl velocity change as compared to the baseline contra-rotating mode. Additionally, the novel mode indicates better low speed power profile and wheel terminal speed as well. Alternative embodiments to enable the co-rotating mode like drilled feed ports and guide vane arrangements are discussed in the work. The hitherto undescribed co-rotating turbine mode operation is unique in its ability to produce and absorb power in the same shaft for bladed turbomachinery. Therefore, purposeful utilization of this mode could enable the design of better, robust, optimized systems for aerospace and energy applications. [DOI: 10.1115/1.4070125]

Keywords: reverse flow, turbine mode, power production, centrifugal compressor, system design

Introduction

In certain cases, it is desirable to operate a centrifugal compressor (CC) as a turbine to produce power in the same shaft through which the CC is driven. This is considered an advantageous proposition in aerospace system architecture designs where:

(1) Shaft power is required only for a miniscule portion of the usage mission profile.

(2) Shaft power output is not necessary at the same time as the CC operation is required.

When such system design requirements exist, the inclusion of a separate turbine to produce power would be a nonoptimal solution. Additionally, such ability to produce power in the same CC drive shaft opens opportunities for designing improved aero systems which combine the functionality of systems that were traditionally addressed separately. Therefore, the consequent system simplification and weight reduction would result in more robust, reliable architectures and improved aircraft mission fuel burn. Architectural system level improvements like these play an important role in the transition to aviation climate neutrality and meet NetZero targets [1].

Turbo Expo: Turbomachinery Technical Conference & Exposition (GT2025), June 16–20, 2025. GT2025.
Manuscript received July 7, 2025; final manuscript received July 24, 2025; published online January 23, 2026. Editor: Jerzy T. Sawicki.

An exemplary application of the use of a CC in turbine mode is in future aircraft environmental control system (ECS). Recent research indicates that ECS variants which include a CC can have fuel burn benefits by 0.5–2% as compared to the conventional two-port bleed system without a CC [2–7]. In the CC-based ECS systems, significant energy savings are obtained by pressurizing the feed air "only" to the cabin requirements. This contrasts with the conventional systems where pressure relief valves are used to regulate high pressure engine bleed air which result in energy loss. One such CC-based ECS system architecture is the engine-mounted cabin compression system (EMC^{2}S) [2]. In this architecture, the fan-bypass air is pressurized by an engine high-pressure shaft driven CC. The total power-off take from the engine is lowered by eliminating high-pressure bleed ports.

The mechanical drive arrangement for the CC in the EMC^{2}S provides synergistic opportunities to utilize the CC in turbine mode to crank the engine shaft during start operation. This would eliminate the need for a separate starting system. During the starting mode, pressurized air from a ground or aircraft source is fed into the outlet of the CC. The high-pressure air then expands through the CC impeller wheel to produce shaft power. This is usually termed as the reverse flow (RF) turbine mode CC operation. The EMC^{2}S architecture in both the forward flow (FF) ECS mode and RF starting turbine mode is shown in Fig. 1. The characteristics and behavior of CC operation in such RF turbine mode have been described in literature and are traditionally represented by the four-quadrant compressor operation map as shown in Fig. 2 [8–12].

The four-quadrant map is constructed by having the flow rate in the horizontal axis and pressure gradient across the compressor in the vertical axis. Forward flow and positive values of pressure gradient and rotation are referred to the nominal compressor operation from the inlet to the outlet. The map demonstrates that power production in the RF turbine mode CC operation during starting will cause the impeller wheel to rotate in a direction opposite to the normal FF ECS operation (RF operation indicated by star in Fig. 2). In this turbine mode operation, the drive shaft is contra-rotating with reference to the nominal ECS mode operation. However, to use the RF turbine mode for cranking the engine, it is necessary that the rotation direction of the shaft connected to the engine should be same in both the ECS and starting modes. Consequently, this would necessitate a complex direction change switch mechanism within the transmission system to rectify the direction of rotation. The direction change mechanism would then need to operate in a complex "asynchronous" manner handling different rotational directions in the input and output shafts. A schematic of the CC operation in the ECS and starting mode indicating the direction change in the CC drive shaft and the direction rectification system to ensure same rotation direction in the engine shaft is shown in Fig. 3. In the reverse flow turbine mode operation, the pressurized air is typically supplied from an external source that is used for engine starting. In this exemplary case, the air from the compressor in the forward flow feeds the ECS air cycle machine and is used cabin conditioning.

A significant improvement in the robustness, reliability, and efficiency of the system can be attained by eliminating the asynchronous, load-carrying, direction change rectification switch. This can be achieved if power can be produced in the CC drive shaft during starting mode in the same direction of rotation as in the ECS mode. In this case, the drive shaft in turbine mode operation will be co-rotating with the ECS mode operation, and the transmission system will operate in a "synchronous" manner handling a single rotational direction. The four-quadrant operating map indicates that co-rotating power production is possible in the fourth quadrant with forward flow and a negative pressure gradient from the inlet to the outlet of the CC. This fourth quadrant, power producing operation is sometimes utilized during compressor start-up with pressurized air supplied at the inlet. However, it is reported from operational experience and experimental investigations that large pressure gradients are required to accelerate the impeller wheel. Moreover, due to these large pressure gradients, operating rotational speeds need to be low to avoid sonic patches in the flow path. On the other hand, the second quadrant, power producing, contra-rotating, reverse flow operation is known to be stable and capable of achieving higher levels of power at higher rotational speeds for lower pressure gradients between the outlet and inlet [8]. Therefore, a new co-rotating, reverse flow power producing mode that is not represented by the conventional four-quadrant map and has the advantages of the stable second quadrant reverse flow operation is required to aid this design improvement. The characteristics and flow physics of this new mode of operation have not been described in literature. A patent has identified the possibility of this new "co-rotating," turbine mode operation, but it does not include any insight into the working and the design principles or the characteristics for such operation [13].

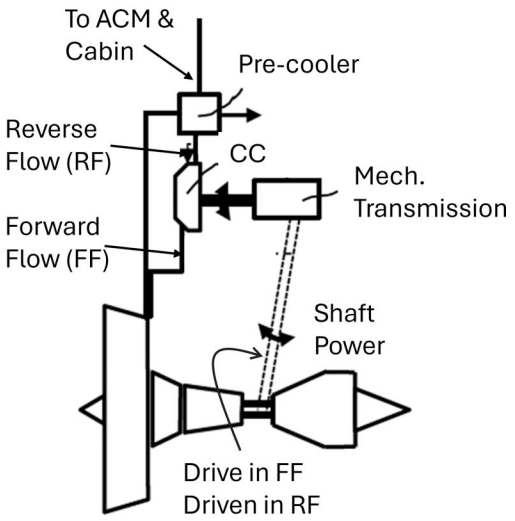

Fig. 1 Schematic of EMC^{2}S architecture showing ECS mode in FF and starting mode in RF

Therefore, this work aims to investigate and describe this novel co-rotating, synchronous, turbine mode CC operation by computationally comparing it with the baseline contra-rotating, asynchronous, turbine mode operation. The work addresses the key research gaps and describes the characteristics of the novel, co-rotating, turbine mode in the following manner:

(1) The baseline second quadrant, power producing reverse flow mode is described in the literature for only axial flow compressors [14]. Therefore, the flow field and operational characteristics of the baseline contra-rotating mode in CC are first described for benchmarking purposes.
(2) The methods required to enable the new co-rotating, turbine mode operation are described. An exemplary configuration in which the diffuser vanes are flipped to point in the opposite direction is discussed in detail to explain the flow physics and key performance metrics. In this case, the impeller nominal suction side would behave like the pressure side in turbine mode enabling co-rotation. Alternative embodiments that feature separate feed ports and vanes are also considered. The design embodiments to enable this operation are filed as patents [15,16].
(3) The reverse flow turbine mode operation in both the co-rotating and the contra-rotating mode is quantified in terms of mass flow handling capacity, power generated, and the peak attainable wheel speed.

Methods

Model Description. The CC design considered for this study is a simplified variant derived from the publicly available NASA High

Efficiency Centrifugal Compressor (HECC) geometry [17]. Several variants of the NASA HECC have been computationally and experimentally investigated. The geometries and the performance characteristics are accessible in the data archive [18]. The NASA HECC represents a state-of-the-art for small CC designs with flow rates and stage total pressure ratios that are in a similar range to CC that may be used for aircraft ECS applications [19–21].

The vaned version of the NASA HECC that features 15 sets of main and splitter blades and 20 sets of main and splitter diffuser vanes is considered in the study. The key turbomachinery design parameters of the NASA HECC are shown in Table 1 [17]. The baseline geometry of the NASA HECC includes a deswirler vane blade row after the diffuser vanes. The deswirler vanes form an axial blade row after the radial portion of the CC to straighten the flow. These are not included in the model for this study as the CC used in ECS does not feature radial to axial transitions in the flow path. Additionally, the splitter blades and vanes are also not included to simplify the model. The simplified CC design is computationally characterized for its performance in the forward flow mode at 100% design speed. At the design point, the simplified design without the splitter and the deswirler vanes indicate 9.5% lower pressure ratio and 6% lower total-to-total adiabatic efficiency than the reported HECC values. The differences represent a good compromise between accuracy and model simplification for the purposes of this study. Moreover, the removal of the splitter blades will not tie down the reverse flow characteristics in the turbine mode operation to the specific geometric features of the HECC, but instead give a generic description of the reverse flow behavior. This is because the details of the local blade geometry and the splitters that are finely tuned for forward flow operation will not significantly affect the performance when the flow direction is reversed. The simplified CC design for the study is shown in Fig. 4.

Domain Discretization and Computational Schematics. Three-dimensional (3D) Reynolds–averaged Navier–Stokes (RANS) simulations are utilized to computationally explore the reverse flow behavior in both the baseline contra-rotating and the new co-rotating turbine mode operation. The computational model of the CC design is divided into three domains: the inlet domain—upstream of the impeller in the nominal operation, the impeller wheel domain, and the diffuser vane domain. Structured, multiblock grids with combined H/J-O topology are used to discretize the domains. Stringent grid quality metrics following best practice guidelines are ensured throughout the computational domain by retaining a minimum face angle of 28 deg and maximum element volume ratio of 3.65. The near wall elements are refined to capture flow gradients. Rounded grid topology is used in the leading edge (LE) and the trailing edge (TE) to better resolve the flow field at different angles. A single periodic passage of the computational

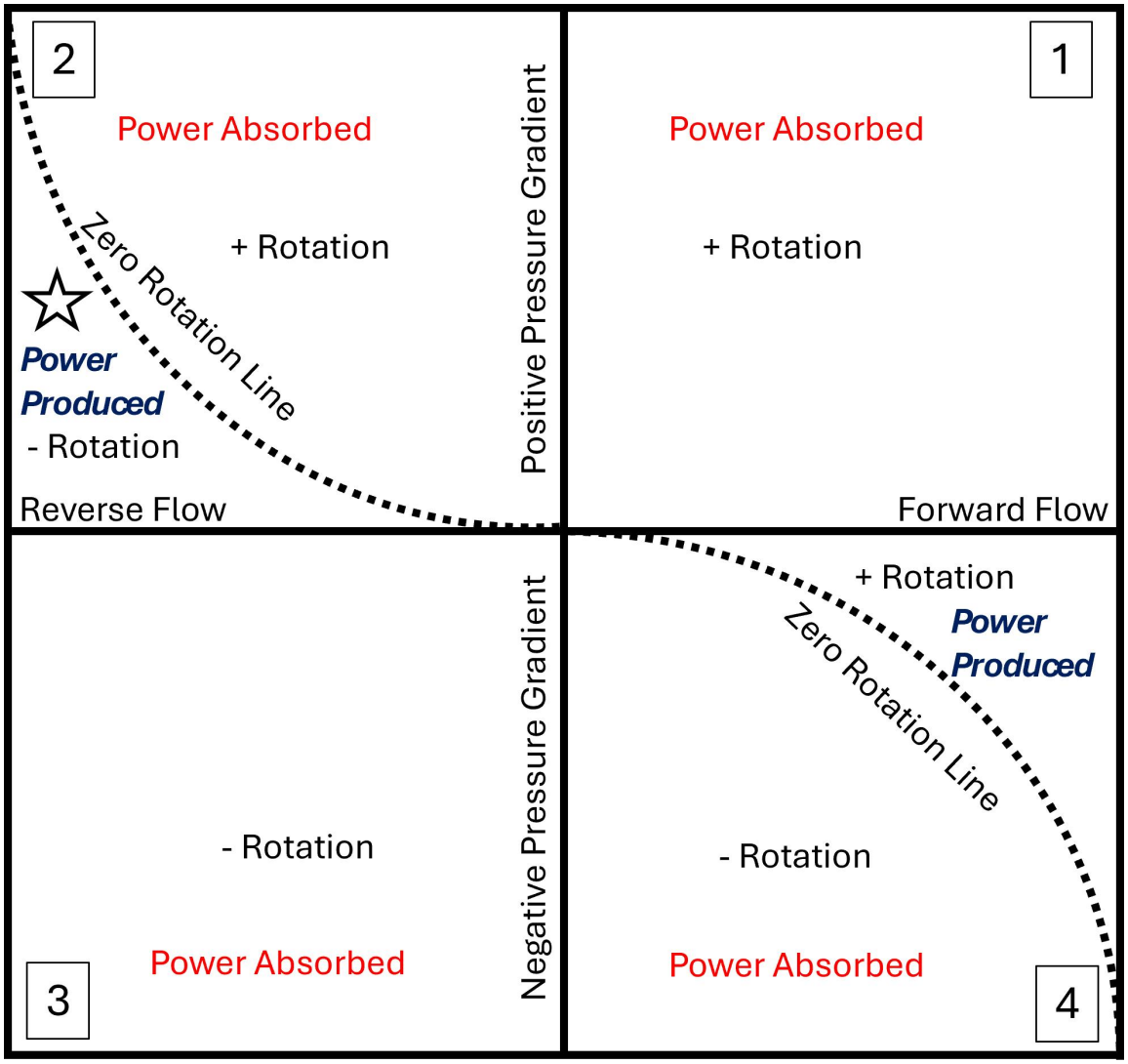

Fig. 2 Representative four-quadrant compressor operation map. Image reconstructed as adapted from Ref. [8].

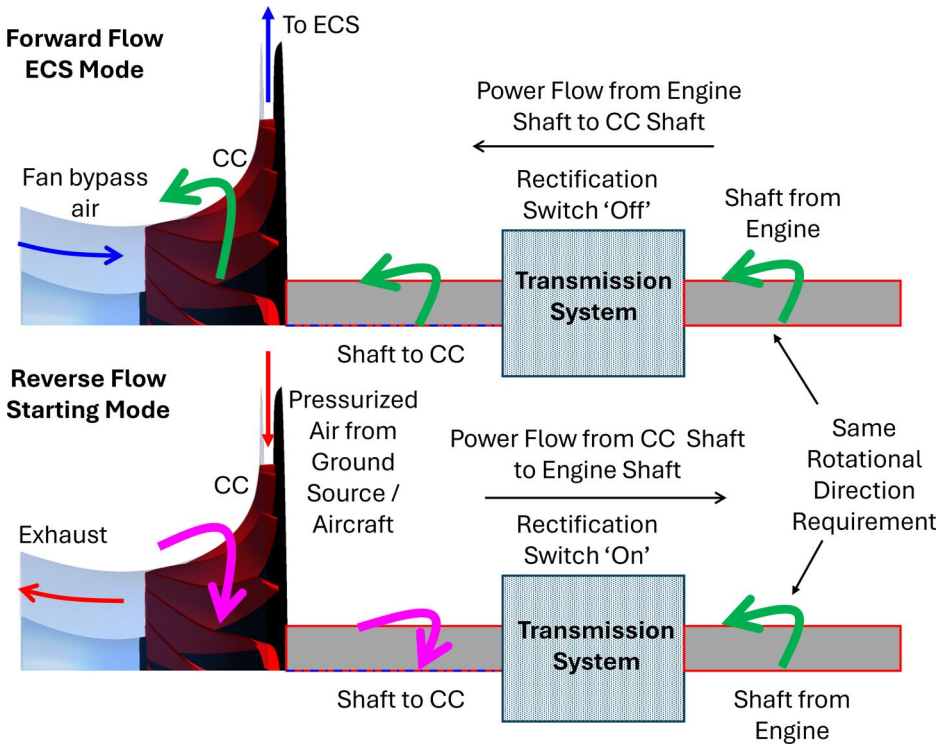

Fig. 3 Schematic showing direction change in the CC shaft during ECS and starting modes

model contains $\sim 0.5 \times 10^6$ elements. This is beyond the conventional requirements for the grid size to be in the zone of asymptotic global parameter change with grid element size. The details of the representative grids are shown in Fig. 5.

In the reverse flow mode, the diffuser vane outlet is specified as the inflow boundary, and the inlet domain ahead of the impeller wheel is specified as the outflow boundary. Total pressure and total temperature are specified at the inflow boundary, and average static pressure is specified at the outflow boundary. The total pressure–static pressure inflow–outflow boundary condition combination is chosen because the mass flow handling capacity in reverse flow is one of the key variables that influence the power produced. A total-to-static pressure ratio of 2 is specified across the CC in reverse flow mode to mimic the typical on-board or ground pressurized air source. Additionally, a pressure ratio of 2 is above the critical choking pressure ratio for air and represents the maximum possible power that can be generated in the reverse flow mode. A single periodic passage of the diffuser vane and the impeller wheel are simulated. The impeller vane is specified as a rotational domain with rotational speed varying from 1% to 100% in steps of 10% for both the baseline contra-rotating and the new co-rotating modes. The steps are defined to mimic the acceleration of the wheel with the constant pressure ratio across the CC in reverse flow. The diffuser vane is as a stationary domain, and a frozen rotor frame change model is used at the interface. Adiabatic, no-slip condition is specified at the stationary and rotating walls.

The flow field solutions to the 3D RANS equations are obtained using a finite-element based, finite volume approach in ANSYS CFX [22]. The RANS equations are solved in a coupled manner using an implicit approach. Higher order spatial resolution schemes are used to reduce dissipative errors in the solution. Turbulence closure is modeled by utilizing two-equation k–ω shear stress transport modeled as in typical centrifugal turbomachinery analysis practice. A parametric convergence criterion with a threshold of less than 0.1% change with pseudo-time step and a discretized equation maximum residual value of 1×10^{-4} is used for terminating the solution algorithm. The computations are carried out in a high-performance computing facility, DELTA 2, using a platform

Table 1 Key features of NASA HECC [17]

Parameter	Value
Design pressure ratio	4.85
Exit corrected mass flow (lbm/s)	2.98
Polytropic efficiency (%)	88.8
Design rotational speed (RPM)	21,789
Impeller tip diameter (in)	16.998
Vaned diffuser outlet diameter (in)	22.398
Work factor ($\Delta H/U_{tip}^2$)	0.79
Diameter ratio at inlet (D_h/D_t)	0.376
Impeller exit blade height (in)	0.609

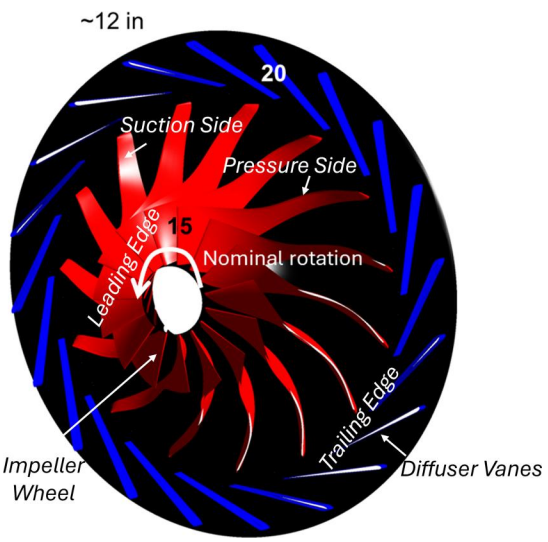

Fig. 4 Simplified CC design adapted from the NASA HECC design showing the nominal rotation direction

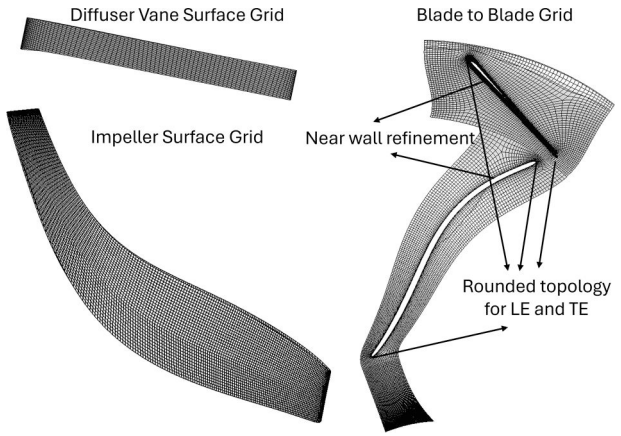

Fig. 5 Representative grids used in the analysis with key features highlighted

message passing interface for parallelization. The 128 cores out of a total of 4096 available cores, with a peak processing power of 60 Teraflops, are used for the simulation. The solutions are carried out in series to mimic the acceleration of the impeller wheel by cascading the results of the current rotational speed to the next higher rotational speed. The full acceleration profile for a single operating mode requires a computational time of ∼12 h.

Designs for Enabling New Co-Rotating Turbine Mode. The baseline contra-rotating mode with reverse flow in the CC design shown in Fig. 4 will rotate in a direction opposite that of the nominal rotation direction. This is because the diffuser vanes direct the flow onto the impeller wheel *pressure* side near the trailing edge regions. Thereafter, the flow expands within the impeller passages and leaves the leading edge in the same direction as the nominal rotational speed vector. Consequently, the efflux direction also aids in the impulse to rotate in the opposite direction during reverse flow operation. On the other hand, to make the impeller wheel rotate in the same direction as the nominal operation, an appropriate mechanism to direct the flow onto the impeller wheel *suction* side is necessary. In such a case, the impulse to rotate will be initiated by the flow impingement by the appropriate flow directors on the suction side.

A possible solution for such a flow director mechanism is to rotate the diffuser vanes by 45 deg in the anticlockwise direction in such a way that it points to the impeller wheel suction side as shown in Fig. 6. In cases where the number of diffuser vanes would cause an entanglement during vane rotation, alternatives to simple rotational pivot mechanisms like a translating vane array assembly could be used. In the translating vane array arrangement, two separate blade rows: the diffuser vane blade row for forward flow CC operation and a separate 45 deg rotated diffuser vane row—termed the nozzle guide vane row for turbine mode, could be included. Depending upon the mode of operation, the appropriate blade row could be retracted and translated into position [16]. In vaneless architectures, the director vanes in turbine mode operation could be deployed into position by rotation along seam pivots. In nominal operation, these director vanes would be flush stowed plates on the vaneless diffuser back plate as shown in Fig. 7. Any other suitable mechanical arrangement to deploy the director vanes can be considered to enable this operating mode.

Alternatively, any other swirl inducing mechanism that will cause flow impingement on the impeller wheel suction side can also be used. Two exemplary arrangements that feature feed ports and guide vanes are considered in this study. In the feed port arrangement, several holes are drilled in the regions above the impeller wheel. These holes are aligned with a radial and tangential swirl angle to cause impingement on the impeller suction wheel. A parametric study to identify the effect of the number of holes and the angle of injection is carried out to identify an optimal configuration. An optimal configuration that maximizes power production with 45, 1 cm diameter holes at 60 deg swirl angle and 30 deg radial angle with 1 cm depth is shown in Fig. 8.

In the guide vane arrangement, a dedicated inlet port for reverse flow is designed just above the impeller wheel before the diffuser vane. This inlet port can be in the shroud—front side of the impeller or hub wall—rear side of the impeller (as in the feed port position). The guide vanes include a swirl angle to direct flow onto the impeller suction side and a radial angle. A design space exploration study is carried out to identify the relative benefit of the rear or front location, swirl angle, and the radial angle. An optimal configuration for maximum power production with the guide vanes in the rear wall, at a 70 deg swirl angle and 30 deg radial angle, is shown in Fig. 9.

In each of the design embodiments to enable the new co-rotating turbine mode operation, the impeller wheel discretized computational domain remains the same. The diffuser vane domain for the 45 deg rotated configuration is regenerated and discretized using structured multiblock grids as in the baseline configuration. Similarly, in the alternative feed port and guide vane arrangements, the diffuser domain is integrated with the feed port or the guide vane. The diffuser vanes are not included for exploring the reverse flow behavior in the alternative embodiments. This is because the diffuser vanes are upstream of these design features and will not influence the

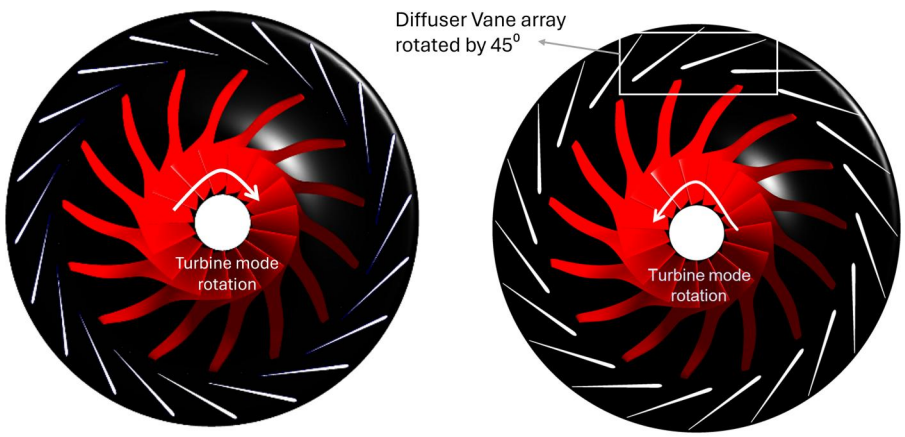

Fig. 6 CC design showing (*a*) baseline contra-rotating turbine mode and (*b*) novel co-rotating turbine mode with flipped vanes

flow development. In all the cases, similar discretization metrics and equivalent grid element sizes are utilized to enable robust comparison without grid difference induced uncertainties. In the rotated diffuser vane configuration, the same total-to-static pressure ratio boundary condition as in the baseline contra-rotating mode is used. In the alternative configurations, the total pressure is specified at the feed port or the guide vane entry instead of the nominal diffuser outlet to mimic pressurized air feed through these features. All configurations in both the baseline contra-rotating mode and in the novel co-rotating mode are run for the same choked total-to-static pressure ratio. Additionally, the effect of the design embodiments on the forward flow is explored at the design point. For the case of the rotated diffuser vane, the effect on forward flow will be due to the tip or hub clearances required for enabling rotation. And in the case of the alternative embodiments, the feed port and guide vane are cavities in the diffuser end wall, which need to be negotiated by the flow leaving the impeller trailing edge in forward flow. The key metrics that are used to describe the reverse flow turbine mode operation are: (1) mass flow handling capacity in reverse flow, (2) power produced at each rotational speed as the impeller wheel accelerates, and (3) peak power and the rotational speed at which it occurs. The peak power rotational speed will be near the terminal speed that the accelerating impeller wheel will sustain during the transient operation. The forward flow effects are characterized in terms of reduction in pressure ratio, mass flow, and efficiency at the design point. Limited unsteady RANS analyses are carried out to identify if the alternative arrangement cavities induce undesirable flow oscillations.

Results and Discussion

To describe and characterize the novel co-rotating, reverse flow turbine mode operation, this section is organized in the following manner:

(1) The baseline contra-rotating, asynchronous reverse flow turbine mode operation is described in terms of the flow field and performance metrics. The physics associated with power production and the available parameters for augmentation are discussed in detail.
(2) The novel co-rotating, synchronous reverse flow turbine mode operation with the flow directors—45 deg rotated diffuser vane configuration—is discussed by describing the flow field and performance metrics. The key differences from the baseline contra-rotating mode and the way power is produced in this counterintuitive operational mode are described by examining the key parameters. This explains the working and design principles of this mode of operation.
(3) The performance metrics and flow field in the novel co-rotating turbine mode for the alternative design embodiments of the feed port and guide vane are discussed. Insights into the effect of design parameters on the extent of power production possible are discussed.

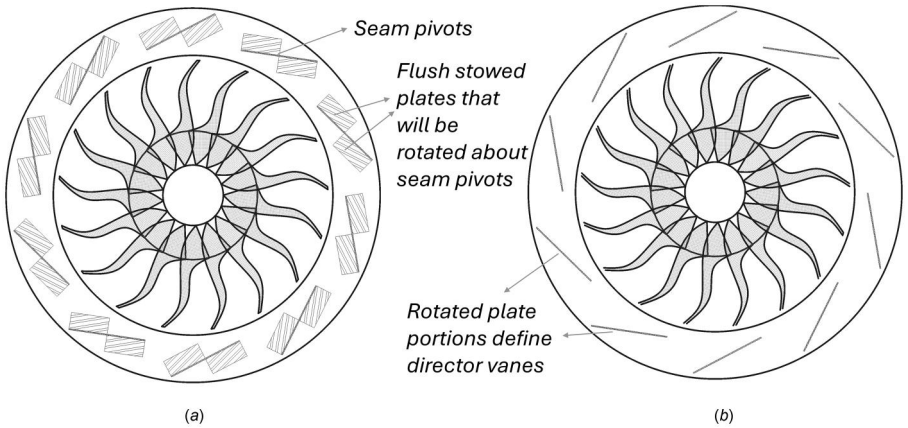

Fig. 7 Exemplary mechanical arrangement for deploying director vanes in vaneless architectures: (*a*) vaneless architecture with director vanes stowed and (*b*) director vanes deployed for co-rotating turbine mode operation

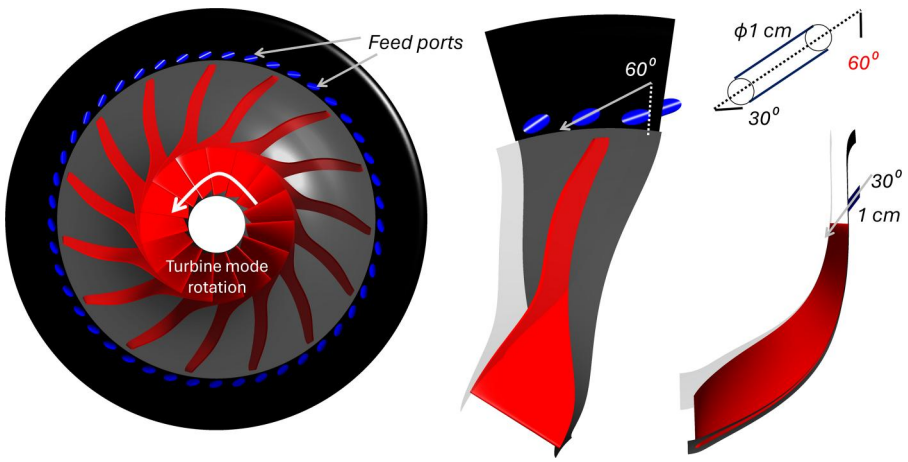

Fig. 8 Feed port arrangement with directed holes to enable co-rotating turbine mode operation

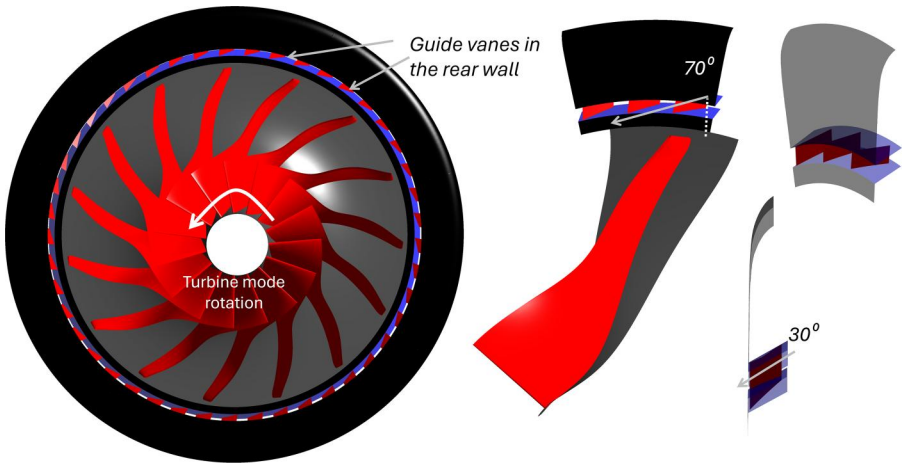

Fig. 9 Rear wall guide vane arrangement to enable co-rotating turbine mode operation

(4) The impact on forward flow due to the design features that are required to enable the co-rotating turbine mode operation is quantified.
(5) An experimental campaign for testing the baseline contra-rotating mode is included for validating the results and providing confidence on the power values reported in the co-rotating mode.

Baseline Contra-Rotating Asynchronous Turbine Mode. The reverse flow, contra-rotating turbine mode is enabled by feeding pressurized air from the nominal CC outlet without any geometric design change. In the nominal forward flow mode, the CC will rotate from the impeller suction to pressure side by absorbing power from the shaft to pressurize the air from the nominal inlet to the outlet. The same CC without any design changes will rotate from the impeller pressure to suction side with reverse flow fed into it from the outlet. The reverse flow expands through the impeller wheel, resulting in a pressure reduction from the outlet to the inlet to produce power. The expansion of the flow through the impeller wheel causes it to accelerate. The flow field across the impeller for a total-to-static pressure ratio of 2, representative of the choked flow through the CC as the impeller wheel starts to accelerate, is used to describe the flow physics during reverse flow operation. Figure 10 shows the projected surface streamlines on a blade-to-blade plane at 50% spanwise height through the diffuser and the impeller wheel at different

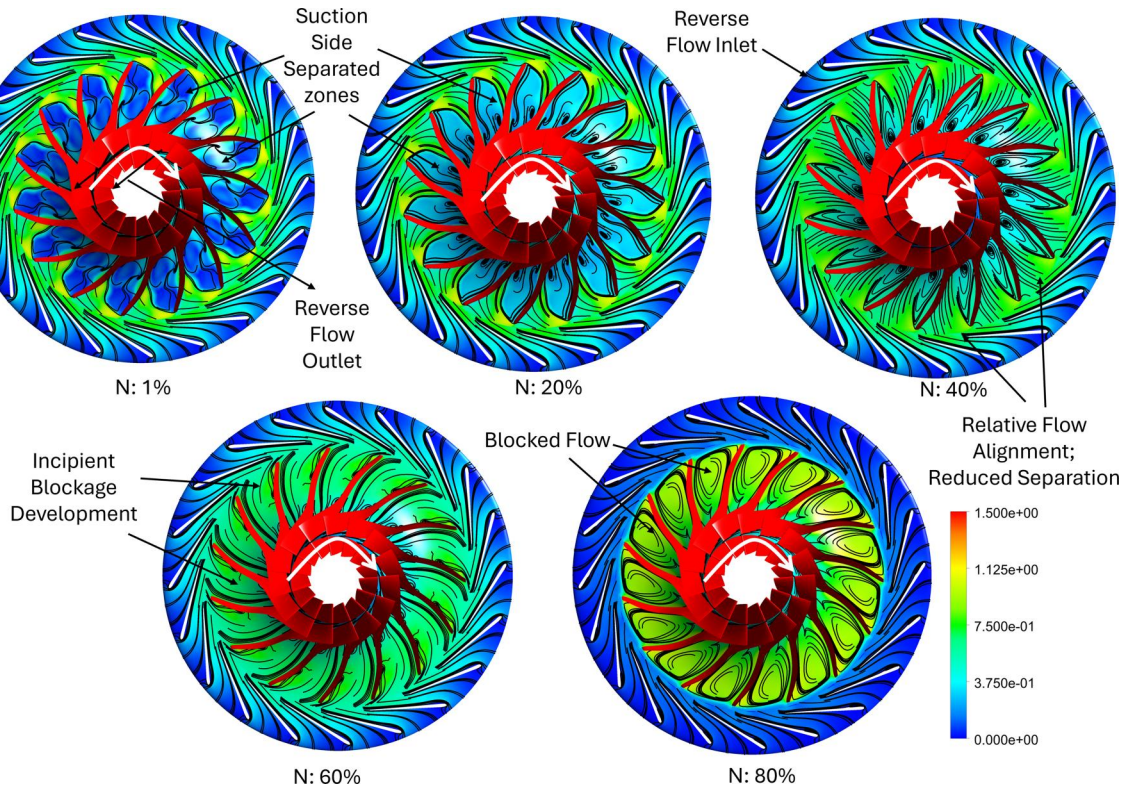

Fig. 10 Streamlines on the 50% blade-to-blade section colored with a Mach number color palette for different rotational speeds in the baseline contra-rotating turbine mode—rotation direction marked in white arrows. Note on color bar—Red does not occur in contours. Impeller is colored red for contrast.

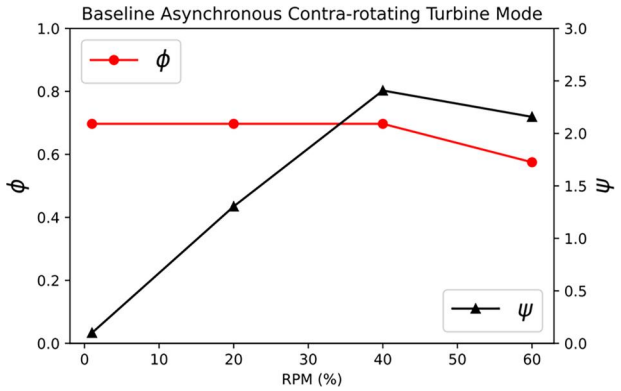

Fig. 11 Flow and power coefficient profile with impeller wheel speed in baseline contra-rotating turbine mode

rotational speeds. The streamlines are overlaid on the Mach number contours; the direction of the streamlines and the Mach number values are relative in the rotating frame.

It is observed from Fig. 10 that as the pressurized reverse flow is fed into the nominal outlet, the diffuser vanes direct the flow onto the impeller wheel pressure side and gives it an impulse to rotate from the pressure side to the suction side. The flow swirl induced due to the diffuser vanes results in a large separation zone that completely covers the suction side of the impeller wheel as can be seen at N:1%. As the flow expands within the impeller passages, the wheel accelerates which results in a change in the relative velocity vector onto the impeller trailing edge. This results in a relative re-alignment of the flow with reference to the impeller trailing edge and results in a reduction in the size of the separation zone progressively, as can be observed at N:20% and N:40%. If the rotational speed was to increase further, it will lead to an incipient blockage development due to the relative velocity vector beginning to align toward the pressure side, as can be seen at N:60%. Further acceleration would result in the incipient blockage zone to completely block off the impeller passages, as can be seen at N:80%. As the blockage zone develops, the mass flow passing through the impeller and the power production begins to drop. Therefore, peak power production in the contra-rotating turbine mode will occur before the initiation of the incipient blockage zone. And the drop in the mass flow handling capacity with blockage would result in an impeller terminal speed between the peak power production speed and the incipient blockage appearance speed. This peak terminal speed in the baseline contra-rotating mode is between 40% and 60% of the design speed.

The mass flow profile and power produced as the impeller wheel accelerates is shown in Fig. 11 in terms of the power coefficient and mass flow coefficient. The power coefficient (ψ) and flow coefficient (ϕ) are defined as below:

$$\psi = \frac{100*\text{Power}}{\gamma D_{\text{in}}^2 \text{P}_{\text{in}} \sqrt{\gamma R T_{\text{in}}}} \tag{1}$$

$$\phi = \frac{10*\text{mflow}\sqrt{T_{\text{in}} R}}{D_{\text{in}}^2 P_{\text{in}} \sqrt{\gamma}} \tag{2}$$

where Power is the shaft power, mflow is the mass flow handling capacity in reverse flow, D_{in} is impeller inlet tip diameter, and P_{in} and T_{in} are the reverse flow inlet total pressure and total temperature, respectively. It is observed that the flow coefficient remains constant till N:40%, where the relative velocity vector flow alignment occurs, and then begins to drop with the incipient blockage development, as observed at N:60%. The power coefficient markedly increases with the impeller acceleration due to effective expansion occurring in the impeller wheel as the flow re-aligns and results in a reduction of the suction side separated flow region. The peak power coefficient occurs at N:40% before the mass flow begins to drop due to the pressure side separation zone blockage. The baseline HECC is experimentally characterized in forward flow only down to N:70%. Therefore, the map is extrapolated down to N:40% along a typical working line from the design point to compare with the reverse mass flow and power production values. It is observed that the maximum reverse flow handling capacity is 53% of the forward flow value, and the peak power produced is ~40% of the power absorbed in forward flow at that speed. The produced power is 18% of the rated power of the CC in forward flow.

The physics of power production in the baseline contra-rotating turbine mode is investigated by utilizing the Euler turbine work equation as shown below:

$$\text{Power} = \text{mflow}\,\Delta(rV_{\text{circ0}}) \tag{3}$$

where r is the radius, V_{circ0} is the swirl velocity in the absolute frame, and Δ operator is considered between the impeller wheel outlet and inlet. At N:40%, where peak power production occurs, the velocity triangle at the impeller rotor inlet and outlet is shown in Fig. 12.

In Fig. 12, the numbers in the velocity triangle are the swirl velocities in the absolute and relative frames, and the axial velocity. The direction of the velocity vectors is shown in the inset. It is seen that the absolute swirl velocity drops by 16× due to expansion and direction change across the impeller wheel to result in power

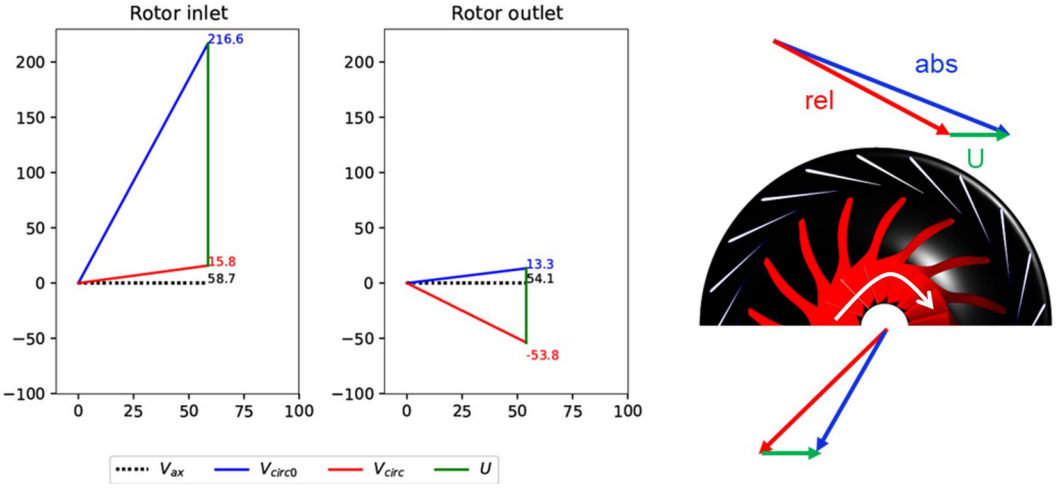

Fig. 12 Rotor velocity triangle at peak power production N:40% in baseline contra-rotating turbine mode. Velocity units in m/s. Positive values in direction of rotation.

production. Equation (3) indicates that to increase the power produced, the value of rV_{circ0} at the reverse flow inlet or impeller outlet is to be greater than the reverse flow outlet or impeller inlet. In the CC impeller wheel, the impeller outlet to inlet radius ratio is 2.92. Therefore, the power production in turbine mode is dominated by the impeller outlet or reverse flow entry absolute swirl velocity and the higher radius at which it occurs. The relative contribution of the impeller wheel inlet or the reverse flow outlet absolute swirl velocity is diminished by the reduction in the radius at the impeller wheel inlet. Therefore, the power production in the turbine mode is influenced by the mass flow handling capacity and the radius weighted change in the absolute swirl velocity.

The power production mechanism provides insight into available parameters for the augmentation of power production capacity in the turbine mode. For instance, the reduction in radius weighted absolute swirl velocity change can be offset by increasing the mass flow through the impeller wheel. To prove this, a notional design with no diffuser vanes and pure radial entry at the impeller wheel outlet for the reverse flow was explored in the contra-rotating mode. The removal of the diffuser vane caused an increase in the flow path throat area as compared to the vaned architecture and resulted in a $\sim 5\times$ increase in the reverse flow handling capacity through the CC. However, since there is no swirl in the impeller outlet, the contribution of the radius weighted change in swirl velocity was reduced by $\sim 4\times$. Consequently, the power production was increased by $\sim 1.3\times$ in this vaneless architecture. Therefore, any suitable design features that either target increased mass flow handling capacity or radius-weighted swirl change need to be optimally chosen for obtaining the desired power production.

Novel Co-Rotating Synchronous Turbine Mode. The exploration of flow field and power production mechanisms in the baseline contra-rotating turbine mode operation provides directions for enabling the counterintuitive co-rotating turbine mode operation. These are:

(1) The necessity of a flow direction mechanism to provide impulse to rotate in the desired direction.
(2) The necessity of flow handling and expansion through the impeller wheel as it accelerates—dictated by the evolution of separated flow features in the impeller passages.
(3) The enabling and optimization of power production by both the mass flow handling capacity and the radius weighted absolute swirl velocity change across the impeller.
(4) The diminishing contribution of the absolute swirl at the impeller inlet or reverse flow outlet due to radius reduction. The radius reduction will dampen the issue due to the direction of the flow leaving the impeller inlet in the same sense as the direction of rotation.

Therefore, with no changes in the baseline impeller wheel geometry and by only the introduction of impulse and swirl generating features at the impeller wheel outlet, the novel co-rotating turbine mode operation can be enabled. As discussed in the methods section, the impulse and swirl generating feature can be the diffuser vanes rotated by 45 deg to direct the flow to impinge on the impeller suction side. The rotated diffuser vanes represent a simple baseline configuration for exploring the novel co-rotating turbine mode operation. The flow field across the CC with the same total-to-static pressure ratio of 2 as in the contra-rotating configuration is shown in Fig. 13. Figure 13 shows the streamlines overlaid on the Mach number contours on the blade-to-blade plane at 50% spanwise height as in the baseline contra-rotating mode operation.

It is observed from Fig. 13 that the pressurized reverse flow now impinges on the suction side and causes it to rotate in the same direction as the nominal CC forward flow operation. The direction of the flow swirl from the diffuser results in a separated flow zone in the pressure side of the impeller passages as can be observed at N:1%. Thereafter, as the wheel starts to accelerate, the re-alignment of the

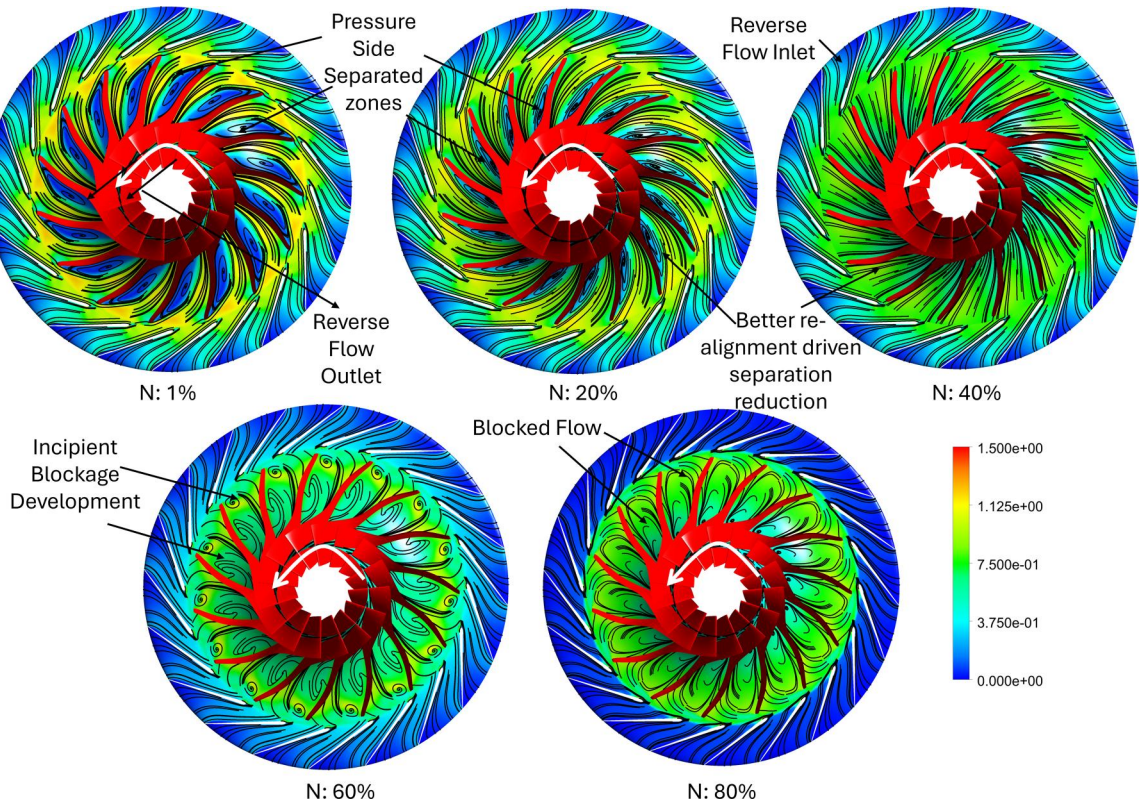

Fig. 13 Streamlines on the 50% blade-to-blade section colored with a Mach number color palette for different rotational speeds in the novel co-rotating turbine mode—rotation direction marked in white arrows. Note on color bar—Red does not occur in contours. Impeller is colored red for contrast.

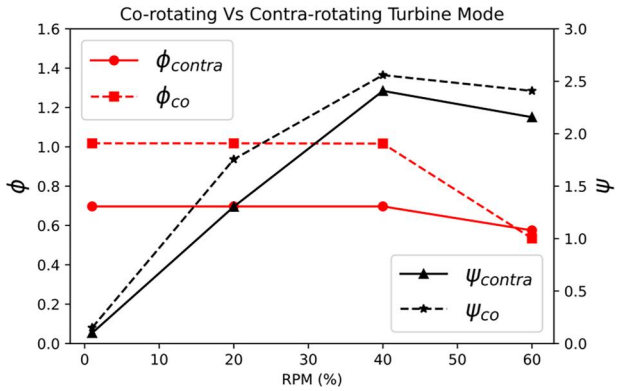

Fig. 14 Comparison of flow and power coefficient profile with impeller wheel speed for baseline contra-rotating and novel co-rotating turbine mode

relative velocity vector with the impeller wheel trailing edge results in a reduction of the separation zone as observed at N:20% and N:40%. Due to the better geometrical alignment of the metal angles at the rotated diffuser outlet and the impeller wheel trailing edge, the extent of the separation zone is smaller, and its size reduces at lower rotational speeds as compared to the baseline contra-rotating operation. As in the baseline contra-rotating configuration, any further acceleration of the impeller results in an incipient blockage region development and subsequent full passage blockage as noticed at N:60% and N:80%. However, this blockage occurs in the suction side in the co-rotating mode rather than the pressure side in the contra-rotating mode. As in the contra-rotating case, the mass flow handling capacity drops after the incipient blockage zone development, and peak power production occurs before this mass flow depletion.

Figure 14 shows a comparison of the mass flow and power production profile in terms of the flow and power coefficients for the baseline contra-rotating and the novel co-rotating configuration. Figure 15 shows the representative velocity triangle at the peak power production speed of N:40% for the novel co-rotating turbine mode.

The maximum reverse flow in the co-rotating turbine mode is 46% higher than the baseline contra-rotating mode. This is because of reduction in the separation zones in the impeller passages due to the better alignment of the diffuser outlet and impeller trailing edge metal angles. However, all this benefit is not translated into the maximum power produced. This is because, as can be observed in the velocity triangle, the reverse flow still leaves the impeller inlet in the same direction as it enters at the impeller outlet. This results in a reduction of flow turning and ~2.5× reduction of absolute swirl velocity across the impeller wheel as compared to the contra-rotating mode. However, the penalty due to the larger residual swirl at the impeller inlet is reduced due to the lower radius at which the reverse flow exits the wheel. Consequently, the radius weighted absolute swirl velocity change term, $\Delta(rV_{circ0})$, is only lower by 16% in the co-rotating configuration as compared to the baseline contra-rotating configuration. The combination of the larger increase in mass flow handling capacity and the relatively lower reduction in radius weighted absolute swirl velocity change results in a 6.25% increase in the peak power production in the co-rotating mode. Additionally, the consistent higher reverse flow handling capacity till the peak power production speed, combined with lower rotational speeds that does not amplify the flow turning change, results in up to 35% higher power at speeds lower than N:40%. Even after the development of the incipient blockage, the co-rotating mode produces 11.6% higher power due to the less deleterious suction side separation as compared to the contra-rotating turbine mode. This stronger acceleration power profile combined with a more graceful depletion beyond peak power production will cause the impeller wheel to attain a higher terminal velocity than the contra-rotating mode. Therefore, the novel co-rotating turbine mode operation not only enables power production for synchronous operation of transmission mechanisms but also could have better performance characteristics than the baseline contra-rotating turbine mode.

Alternative Embodiments for Novel Co-Rotating Turbine Mode. The novel co-rotating turbine mode can be enabled by any suitable swirl inducing mechanisms that can provide the starting impulse for rotation on the impeller wheel suction side. The feed port and guide vane embodiments shown in Figs. 8 and 9, respectively, are exemplary alternative swirl inducing mechanisms to the rotated diffuser vane configuration. In the feed port configuration, several tangential and radially angled holes are drilled after the impeller wheel. Several parametric studies were conducted to identify the combination of tangential and radial angle along with the number of holes for maximizing power production. Figure 16 shows the 3D streamlines during the start of the impeller wheel acceleration at N:1% for a feed port configuration with 45 holes, 60 deg tangential angle, and 30 deg radial angle. The tangential angle choice is a tradeoff between the maximum mass flow handling capacity and the inlet absolute swirl velocity. It is noticed values from 80 deg to 60 deg display similar power characteristics, but any value below

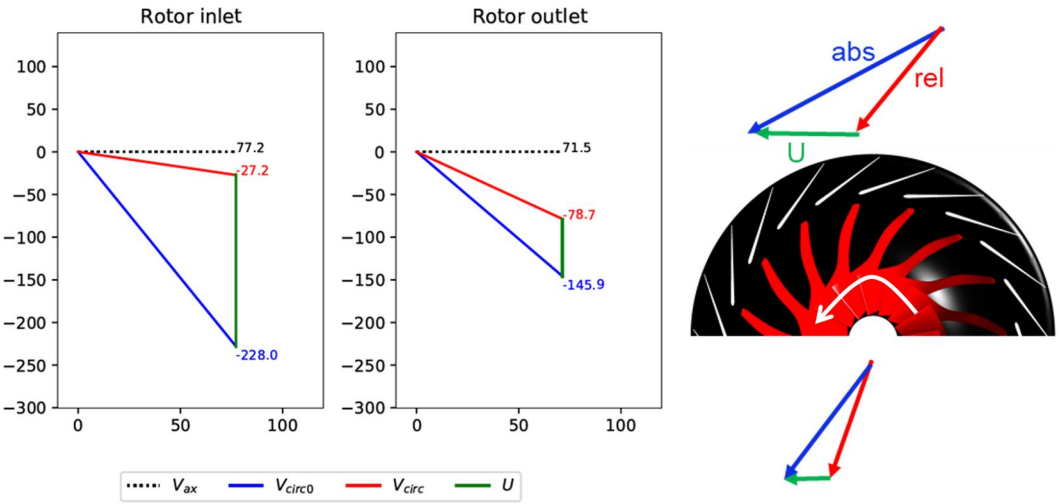

Fig. 15 Rotor velocity triangle at peak power production N:40% in the novel co-rotating turbine mode. Velocity units in m/s. Positive values as in baseline contra-rotating direction.

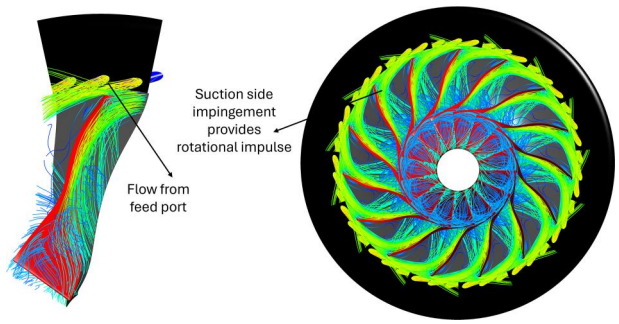

Fig. 16 3D streamlines in the feed port architecture for N:1% in the novel co-rotating turbine mode

60 deg results in a sharp power reduction because of the reduction in the radius weighted inlet absolute swirl velocity value. The radial angle is selected based on optimum impingement on the impeller wheel suction side. This value is found to depend on the impeller wheel back-sweep angle.

In the guide vane embodiment, to maximize the reverse flow fed into the CC wheel, a dedicated inlet port with guide vanes to swirl the flow toward the impeller suction side is considered. Parametric studies on the positioning of the guide vane inlet port indicated that a rearward placement—on the diffuser hub wall—increases the power produced by 13% due to preferential direct impingement on the impeller wheel. Additionally, it was noted that a tangential angle of 70 deg represents an optimal tradeoff between absolute swirl velocity change and mass flow handling capacity. As in the feed port, a radial angle of 30 deg is fixed based on the impeller geometry. The flow field with the guide vane port is like that of the feed port indicating impingement and expansion. The flow field as the impeller accelerates in the alternative embodiments is also like the baseline rotated diffuser vane configuration. The mass flow and power production profile in terms of the flow and power coefficients for the optimized feed port and guide vane architectures, along with the baseline rotated vane configuration in the novel co-rotating, synchronous turbine mode, is shown in Fig. 17.

It is observed from Fig. 17 that the mass flow handled by the guide vane configuration is only 4% lower than the rotated diffuser vane configuration. This is because the effective area available for the guide vane before potential interaction with diffuser vane zone is sufficient to accommodate as much mass flow as the rotated diffuser vane. On the other hand, the discrete hole arrangement in the feed port configuration has 65% lower mass flow than the rotated vane configuration because of the restrictions in available area for drilling

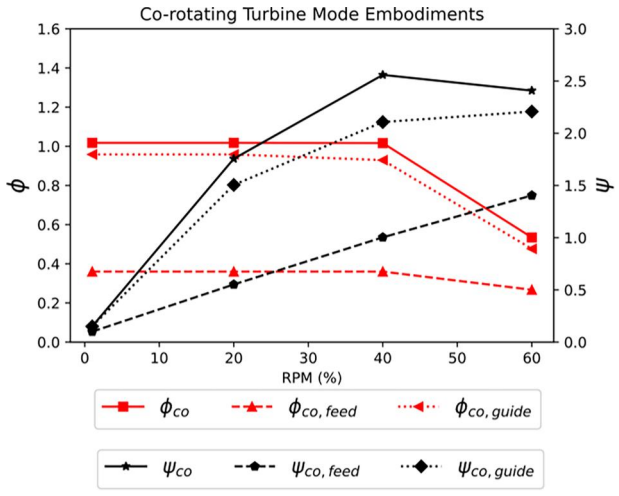

Fig. 17 Comparison of flow and power coefficient profile with impeller speed for novel co-rotating turbine mode embodiments

the holes at the desired radii. Larger holes would interact with each other and the diffuser vane zone. The differences in the mass flow profile are also reflected in the profile of power produced with impeller wheel speed. In all cases, the change in the absolute swirl velocity component is similar because of similar swirl angles at the impeller wheel outlet. Therefore, the power produced by the guide vanes is 13% lower, and the feed port is 45% lower than the rotated diffuser vane configuration. Notably, in both the feed port and guide vane configuration, the peak power is produced at N:60% as compared to N:40% at the baseline rotated configuration. This is because of the minor flow field changes in the impeller wheel due to the impingement of the directed jets with the tip shroud walls before it interacts with impeller blades. This interaction further amplifies the pressure losses and is responsible for the larger reduction in power as compared to the mass flow profile. The peaking of the power at higher impeller wheel speeds alleviates the power loss to a certain extent due to a higher impeller wheel torque at higher speeds. Therefore, it is noted that rotated diffuser vane configuration has better characteristics than the feed port or the guide vane architecture.

A notional configuration without the rotated diffuser vanes but with the same amount of swirl introduced externally indicated a doubling of the power produced as compared to the baseline rotated co-rotating configuration. This is due to a 2.5× increase in the reverse flow due to the removal of the diffuser vane throat restriction and a reduction in the diffuser vane row pressure losses. This notional configuration represents a potential maximum power attainable in the novel co-rotating turbine mode. A similar external swirl inducer without the diffuser vane in contra-rotating turbine mode configuration also exhibited doubling of the baseline power produced due to similar reasons. The streamlines on the blade-to-blade plane at 50% spanwise height for both the co-rotating and contra-rotating modes for this notional potential maximum power production case at N:40% are shown in Fig. 18. Minor improvements over these can be obtained by modulating the swirl angle to match with the impeller acceleration. However, the mechanical design and control requirements for such minor advantages would not justify the minor increments attainable.

Effect of Design Modifications on Forward Flow. The design modifications in the diffuser vane space required to enable the novel co-rotating turbine mode operation would have impact on the forward flow design and optimization of the CC. The rotated diffuser vane arrangement would necessitate mechanisms that would enable rotation and consequently result in tip and/or hub clearances depending upon the mechanical arrangement. Exploratory characterization runs at forward flow design speed line were carried out to quantify the impact of the clearances for 1% (0.005 in) and 2% (0.01 in) tip and hub clearances. It was observed that the 1% tip and hub clearance result in 2.1% increase in choke mass flow, 3% maximum reduction in efficiency, and 3.5% reduction in surge pressure ratio (defined as numerical stall instability boundary). The 2% hub and tip clearance results in 3.8% increase in choke mass flow, 4% maximum reduction in efficiency, and 5.2% reduction in surge pressure ratio. These exchange rates are typical to the values reported in experimental literature for CC [23]. The alternative embodiments of the feed port and the guide vane are recommended to be implemented in such a way that there are ports that will block these potential leakage paths during forward flow operation. However, if such ports are not implemented, the leakage paths would affect the baseline forward flow performance. These leakage paths into a potential distribution plenum of volume 443 cubic inches (25% of the diffuser volume) that run around the periphery of the impeller wheel are modeled in the forward flow quantify its impact. It is observed that the increased losses due to the leakage into the plenum will result in a maximum reduction of efficiency by 2.5% with a maximum leakage flow rate of 13% entering and exiting the plenum. Therefore, it is recommended that a detailed characterization of forward flow behavior with all the design features for the co-rotating

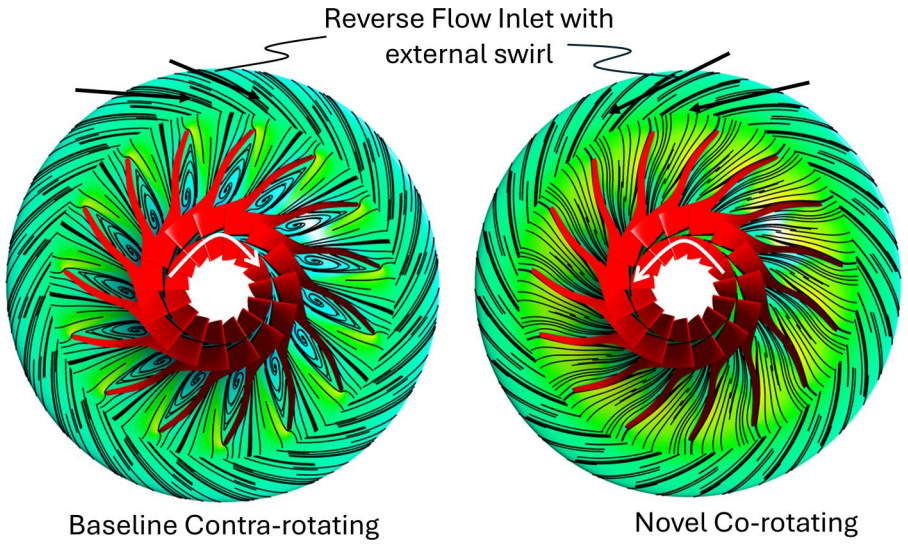

Fig. 18 Notional maximum potential power production case in the contra-rotating and co-rotating mode with externally induced swirl

turbine mode operation be carried out for choosing the appropriate mechanical architecture.

Preliminary Experimental Investigation of Contra-Rotating Mode. A centrifugal compressor test rig with the general layout shown in Fig. 19 was used to test the baseline contra-rotating reverse flow mode. Insets in Fig. 19 show the facility picture and condensate shedding in turbine mode operation. In the nominal forward flow operation mode, ambient air or high-pressure supply air feeds the centrifugal compressor which is driven by a motor through the shafting. In the reverse flow operation mode, air is supplied at the outlet of the compressor through alternative piping as shown in Fig. 19. In the reverse flow mode, the power produced by the CC in turbine mode and the rotational speed are measured from invertors connected to the drive shaft. The CC investigated in the study has similar operating pressure ratios and flow coefficients as the NASA HECC. In reverse flow, the CC will rotate in the contra-rotating mode because no changes were made to the baseline design. The experiment was run with pressurized air at 4 bar supplied at the

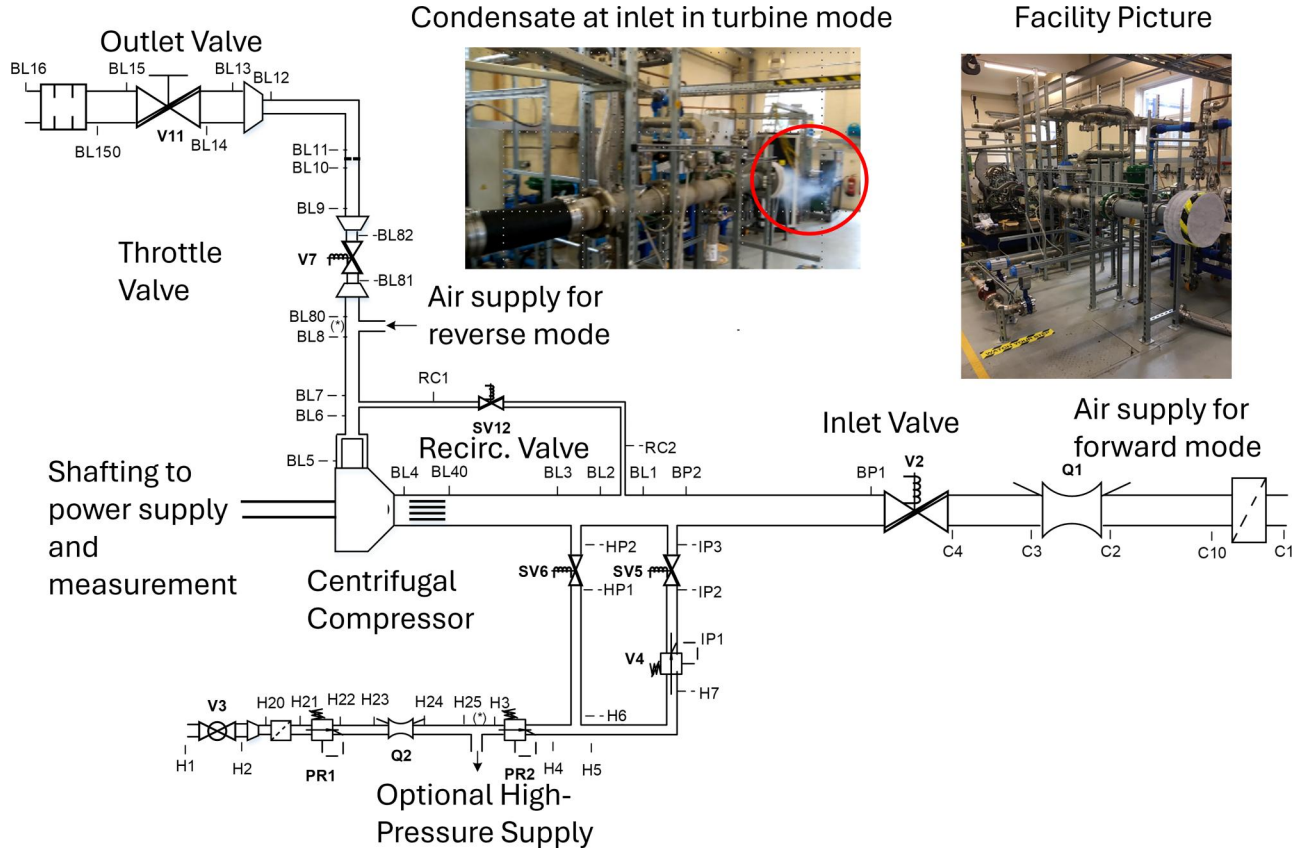

Fig. 19 Experimental facility layout for reverse flow contra-rotating mode investigations. Picture of the facility shown in inset.

outlet and allowed to expand through the CC. In the turbine mode operation, clear indication of condensate shedding out of the inlet pipe was noted, as shown in inset of Fig. 19. It was noted that as the CC impeller reached 35% of the design speed in the contra-rotating turbine mode, the power output was ∼13% of the rated power. 3D RANS analysis of the HECC in the baseline contra-rotating mode at 35% design speed results in ∼16% of the rated power. The differences are attributed to leakages which are not modeled in 3D RANS. These preliminary experimental investigations provide validation to the expected power production profile in the co-rotating mode as well. Detailed experimental investigations in the co-rotating mode in the reverse flow mode will be carried out in the future.

Conclusions

A hitherto undescribed, novel, co-rotating, reverse flow turbine mode in a CC is described along with the methods necessary to enable this operating mode. This novel mode is compared with the expected baseline contra-rotating, reverse flow, turbine mode operation, which is also undescribed in the literature. The CC architecture considered in this study is the NASA HECC design, which is typical of the state-of-the-art design practice. The key outcomes from the study are:

(1) In the baseline contra-rotating turbine mode, the swirl induced by the diffuser vanes generates the rotational impulse by directing reverse flow onto the impeller pressure side and causes it to rotate in the direction opposite to that of nominal forward CC rotation. Thereafter, the expansion of the flow through the wheels results in peak power production of ∼40% of the forward flow value at an impeller rotational speed of 40% of design, and peak terminal impeller speed between 40% and 60%. This peak power is ∼18% of the full rated power in forward flow. The mechanism of power production is dominated by change in absolute swirl velocity through the impeller wheel because the reverse flow through the impeller is compromised due to the large suction side separation.

(2) The novel co-rotating turbine mode can be enabled by any appropriate swirl inducing mechanism that generates rotational impulse by directing flow onto the impeller suction side and thus causes it to rotate in the same direction as the nominal forward CC rotation. In the novel co-rotating mode, the flow exits the impeller at the inlet in the same direction as it enters because of the impeller inlet angle optimized for CC forward flow operation. This results in a lower absolute swirl velocity change in the novel co-rotating mode as compared to the baseline contra-rotating mode. However, this does not significantly impact power production because of the radius decrease across the impeller wheel in CC. This alleviates the flow field impediment due to the radius weighting of the absolute swirl velocity. Moreover, control over the amount of power produced can be exercised through the reverse flow handling capability in addition to swirl change. The reverse mass flow handled in the novel co-rotating mode is higher due to better alignment at the impeller trailing edge due to the optimization of impeller exit angle, often with back sweep, for better forward flow performance.

(3) A design configuration with 45 deg rotated diffuser vanes that direct flow onto the impeller suction side to enable the novel co-rotating turbine mode resulted in 46% more reverse flow than the baseline contra-rotating mode. However, the flow impediment at the inlet resulted in a drop in the radius weighted absolute swirl change by 16%. The combination of both these factors resulted in a 6.25% higher peak power production than the baseline mode at similar impeller wheel speeds. Additionally, the novel co-rotating mode indicates consistently higher power levels of up to 35% till the peak power production speed. Lower power drop after the peak power production indicates that the impeller terminal speed will also be higher than the baseline mode.

(4) Alternative embodiments like drilled feed ports aligned to direct the flow onto the impeller suction side and guide vanes at the impeller wheel outlet have also demonstrated the ability to produce power in the novel co-rotating turbine mode. The guide vane embodiment has power characteristics like the rotated diffuser vane configuration, while the feed port arrangement produced lower levels of power due to restrictions on the amount of flow that can be feed through the ports.

(5) An exemplary case of utilizing the CC used in a novel ECS system in the turbine mode is considered as one of the applications of the novel co-rotating turbine mode to gain system level benefits. The absolute values of power produced in the novel co-rotating mode—the rotated diffuser vane and the guide vane embodiments—can meet the starting requirements demanded by HP spool acceleration in typical gas generators [24,25].

The novel co-rotating turbine mode configuration, as described in this study, is a new mode of CC operation. This mode enables the production and absorption of power in the same shaft, with the same direction of rotation in bladed turbomachinery. Therefore, it is posited that the novel synchronous turbine mode operation will have wider implications for several aerospace and energy systems. Preliminary experimental campaigns have indicated the levels of power reported in the baseline contra-rotating mode are aligned with the values reported in the study. Wider experimental campaigns with the novel co-rotating, turbine mode are being considered for future work.

Acknowledgment

The authors would like to express their gratitude to Rolls-Royce plc. for supporting this research and for permission to publish the paper. The work was carried out under InnovateUK—Aerospace Technology Institute (ATI) Project PINES, Reference No. 113263.

Funding Data

- InnovateUK—Aerospace Technology Institute (ATI) Project PINES (Reference No. 113263; Funder ID: 10.13039/501100000767).

Data Availability Statement

The authors attest that all data for this study are included in the paper.

Nomenclature

D = diameter
H = total enthalpy
mflow = mass flow
N = RPM
P = total pressure
r = radius
R = gas constant
T = total temperature
U = rotational speed
V = velocity
γ = ratio of specific heat constants
Δ = change
Φ = flow coefficient
ψ = power coefficient

Subscripts

ax = axial velocity
circ = relative swirl velocity
circ0 = absolute swirl velocity

co = co-rotating
contra = contra-rotating
feed = feed port
guide = guide vane
in = inlet
rel = relative velocity

Abbreviations

ACM = air cycle machine
CC = centrifugal compressor
ECS = environmental control system
EMC^2S = engine-mounted cabin compression system
FF = forward flow
HECC = High Efficiency Centrifugal Compressor
LE = leading edge
RANS = Reynolds-averaged Navier–Stokes
RF = reverse flow
TE = trailing edge

References

[1] Levin, K., Rich, D., Ross, K., Fransen, T., and Elliott, C., 2020, "Designing and Communicating Net Zero Targets," World Resources Institute, Washington, DC, accessed Dec. 4, 2022, https://www.wri.org/research/ designing-and-communicating-net-zero-targets

[2] van Heerden, A. S., Ippedico, S., Rajendran, D. J., Anselmi-Palma, E., Roumeliotis, I., Pachidis, V., Sharpe, R., and Howarth, N., 2023, "Performance Analysis of an Engine-Mounted Compression System for Aircraft Environmental Control," ASME Paper No. GT2023-100761.

[3] Sinnett, M., 2007, "787 No-Bleed Systems: Saving Fuel and Enhancing Operational Efficiencies," Aero Q., **18**, pp. 6–11.

[4] Jiang, H., Dong, S., and Zhang, H., 2016, "Energy Efficiency Analysis of Electric and Conventional Environmental Control System on Commercial Aircraft," 2016 IEEE International Conference on Aircraft Utility Systems (AUS), Beijing, China, Oct. 10–12, pp. 973–978.

[5] Parrilla, J., 2014, "Hybrid Environmental Control System Integrated Modeling Trade Study Analysis for Commercial Aviation," Dissertation, University of Cincinnati, OH.

[6] Peng, X., 2013, "Aircraft Environmental Control Systems Modeling for Configuration Selection," M.Sc. thesis, Cranfield University, Washington, DC.

[7] Linares, D. P., 2016, "Modeling and Simulation of an Aircraft Environmental Control System," Ecole Polytechnique, Montreal, QC, Canada, https://publications.polymtl.ca/2277/1/2016_DanielPerezLinares.pdf

[8] Gill, A., Von Backström, T. W., and Harms, T. M., 2007, "Fundamentals of Four-Quadrant Axial Flow Compressor Maps," Proc. Inst. Mech. Eng., Part A: J. Power Energy, **221**(7), pp. 1001–1010.

[9] Belardini, E., Rubino, D. T., Tapinassi, L., and Pelella, M., 2016, "Four Quadrant Centrifugal Compressor Performance," Asia Turbomachinery & Pump Symposium, Singapore, Feb. 22–25, pp. 1–9.

[10] Serena, A., and Bakken, L. E., 2023, "Experimental Characterization of a Centrifugal Compressor in Second Quadrant Operation," ASME Paper No. IMECE2023-112735.

[11] Pronk, O. I., and Bakken, L. E., 2024, "Experimental Characterisation of Surge Cycles and Second Quadrant Operation for a Centrifugal Compressor," ASME Paper No. GT2024-121338.

[12] Serena, A., and Bakken, L. E., 2024, "Transient Analysis of Flow Unsteadiness and Machine Instabilities in a Centrifugal Compressor at Surge and Second Quadrant Operation," ASME Paper No. GTP-24-1645.

[13] Hidefumi, S., 2014, "Turbine Compressor Device, Turbine Compressor System, and Aircraft Ventilation System," Patent No. WO2014020770A1.

[14] Gill, A., Von Backström, T. W., and Harms, T. M., 2012, "Reverse Flow Turbine-Like Operation of an Axial Flow Compressor," ASME Paper No. GT2012-68783.

[15] Murray, C. A., Howarth, N., Swain, D., and Bousfield, I. J., 2023, "Blower System," U.S. Patent Application 18/155,351.

[16] Murray, C. A., and Howarth, N., 2024, "Rotary Assembly," U.S. Patent Application 18/379,976.

[17] Medic, G., Sharma, O. P., Jongwook, J., Hardin, L. W., McCormick, D. C., Cousins, W. T., Lurie, E. A., Shabbir, A., Holley, B. M., and Van Slooten, P. R., 2014, "High Efficiency Centrifugal Compressor for Rotorcraft Applications," National Aeronautics and Space Administration, Washington, DC, Report No. NASA/CR-2014-218114.

[18] Harrison, H. M., 2024, "NASA High Efficiency Centrifugal Compressor Data Archive,".

[19] Robles Vega, G., Bosshart, A. J., Ni, M., Ni, R. H., Harrison, H. M., and Nguyen-Huynh, T., 2024, "NASA HECC Geometry and Performance Review Part 1: Validation of a Computational Model for the Vaneless Diffuser Configuration With As-Manufactured Impeller Geometry," ASME Paper No. GT2024-125128.

[20] Robles Vega, G., Bosshart, A. J., Ni, M., Ni, R. H., Harrison, H. M., and Nguyen-Huynh, T., 2024, "NASA HECC Geometry and Performance Review Part 2: Geometric Differences Between the As-Manufactured and Design-Intent Impeller Geometry and Their Effects on the Vaneless Diffuser Configuration Performance," ASME Paper No. GT2024-125360.

[21] Harrison, H. M., Nguyen-Huynh, T., and Mathison, R. M., 2024, "NASA HECC Geometry and Performance Review Part 3: A Numerical and Experimental Investigation of Tip Clearance Effects on the Vaneless Diffuser Configuration," ASME Paper No. GT2024-121641.

[22] ANSYS Inc., 2024, *ANSYS CFX, Release 2024R1, CFX-Solver Theory Guide*, ANSYS, Canonsburg, PA.

[23] Ubben, S., and Niehuis, R., 2015, "Experimental Investigation of the Diffuser Vane Clearance Effect in a Centrifugal Compressor Stage With Adjustable Diffuser Geometry—Part I: Compressor Performance Analysis," ASME J. Turbomach., **137**(3), p. 031003.

[24] Agrawal, R. K., and Yunis, M., 1981, "A Generalized Mathematical Model to Estimate Gas Turbine Starting Characteristics," ASME Paper No. 81-GT-202.

[25] Wang, Z., Zhang, J., Gao, C., and Ming, L., 2023, "Effect of Air Properties on a Twin-Shaft Turbofan Engine Performance During Start-Up," Appl. Therm. Eng., **218**, p. 119387.

On a novel co-rotating synchronous turbine mode operation in a centrifugal compressor

Rajendran, David John

2026-03

Rajendran DJ, Palma EA, Roumeliotis I, et al., (2026) On a novel co-rotating synchronous turbine mode operation in a centrifugal compressor. Journal of Engineering for Gas Turbines and Power, Volume 148, Issue 3, March 2026, Article number 031027

https://doi.org/10.1115/1.4070125